

## Tuning the Conductivity of Polyaniline through Doping by Means of Single Precursor Vapor Phase Infiltration

*Weike Wang, Fan Yang, Chaoqiu Chen, Lianbing Zhang, Yong Qin\* and Mato Knez\**

W. Wang, F. Yang, Dr. C. Chen, Dr. M. Knez  
CIC nanoGUNE, Tolosa Hiribidea, 76, 20018 Donostia-San Sebastian, Spain

E-mail: [m.knez@nanogune.eu](mailto:m.knez@nanogune.eu)

W. Wang, Dr. C. Chen, Dr. Y. Qin

State Key Laboratory of Coal Conversion, Institute of Coal Chemistry, Chinese Academy of Sciences, Taiyuan, 030001, China

E-mail: [qinyong@sxicc.ac.cn](mailto:qinyong@sxicc.ac.cn)

W. Wang, University of Chinese Academy of Sciences, Beijing, 100049, China

Dr. L. Zhang, School of Life Sciences, Northwestern Polytechnical University, Xi'an, 710072, China

Dr. M. Knez, IKERBASQUE, Basque Foundation for Science, 48011 Bilbao, Spain

Keywords: vapor phase infiltration, single precursor, conductivity, polyaniline, doping

The present work describes a novel single precursor vapor phase infiltration (VPI) process to dope polyaniline (PANI). The infiltration was performed with the metal containing atomic layer deposition (ALD) precursors  $\text{MoCl}_5$  or  $\text{SnCl}_4$ . The conductivities were assessed with four-point probe measurements and showed significant enhancements by up to 6 orders of magnitude, confirming the efficiency of the VPI process. Furthermore, we found that the conductivities of PANI/ $\text{MoCl}_5$  and PANI/ $\text{SnCl}_4$  outperform the conductivity of HCl doped PANI if exposed to elevated temperatures (150 °C) in vacuum. The chemical changes resulting from the infiltration of PANI were characterized applying FTIR and Raman spectroscopy. SEM micrographs showed that the morphologies of the samples did not alter after the infiltration process.

### 1. Introduction

Conductive polymers are subject of research since several decades, but their promise as functional material in flexible electronics seriously intensified the research effort on those

materials during the past years. Improvement of the conductivity and chemical or thermal stability of a conductive polymer will allow beneficial substitution of inorganic materials in a broad range of electronic devices, including thin-film transistors,<sup>[1]</sup> light emitting diodes,<sup>[2]</sup> solar cells,<sup>[3]</sup> batteries,<sup>[4]</sup> or supercapacitors.<sup>[5]</sup> With its highly conjugated  $\pi$  delocalized molecular backbone, Polyaniline (PANI) belongs to the most prominent organic semiconductors and acts as model system for many further conductive polymers. With view on its application potential, very promising results have been demonstrated in a variety of application fields including sensors, actuators, antistatic coatings, corrosion protection, rechargeable batteries, microwave absorption and electro-optic and electrochromic devices.<sup>[6,7]</sup> The level of conductivity of PANI is of crucial importance for most of the applications and depends on the switching between the different states of the polymer, namely, leucoemeraldine, emeraldine, and pernigraniline states, as a response to a chemical or electrical trigger. The conductivity of PANI can be altered by doping and inorganic protonic acids,<sup>[8,9]</sup> organic acids,<sup>[10,11]</sup> alkali metal salts,<sup>[12,13]</sup> lewis acids,<sup>[14,15]</sup> and transition metal salts<sup>[16,17]</sup> are the most commonly used dopants. Usually, the doping relies on wet chemistry, which not only introduces impurities into the PANI by inclusion of solvent molecules or additives, but also severely influences the morphology and structure of PANI as such additives impact the polymerization or crystallization of the material. This is very often considered to be a serious drawback for shaping the polymer for various applications. A promising approach to avoid such negative influence from the solvents and obtain better control of the doping process may lie in vacuum-based processing. In fact, atomic layer deposition (ALD) and related vapor phase infiltration strategies take advantage of the mobility of a vaporized chemical to diffuse into and react with polymeric substrates,<sup>[18]</sup> which may be very beneficial for a solvent-free and controllable doping process.

Incorporation of inorganic materials into polymers often enhances the mechanical, optical, or electronic properties of the resulting composite or hybrid material.<sup>[19-26]</sup> For example, in our

earlier works we have demonstrated that infiltration of metal oxides or metal ions into various (bio)polymers, including spider silk,<sup>[24]</sup> avian egg collagen<sup>[25]</sup> and cellulose<sup>[26]</sup> by means of ALD-derived strategies often results in hybrid materials with exceptional mechanical properties. In the present work, we demonstrate that a similar infiltration process can also be used for doping PANI. The strategy further allows for controlling the level of conductivity of the polymer through the number of infiltration cycles applied. After doping with metal chlorides, the doped PANI shows exceptional conductivity values, particularly at elevated temperatures, indicating a significant difference in the physics and chemistry of the material in comparison to PANI doped in a traditional way. On the example of two different ALD precursors, MoCl<sub>5</sub> and SnCl<sub>4</sub>, we demonstrate that the conductivities of the resulting PANI/MoCl<sub>5</sub> and PANI/SnCl<sub>4</sub> are superior to those of PANI doped with 1M HCl after exposure to elevated temperatures (150 °C). This method may serve as complementary route for stabilizing conductive PANI for high-temperature applications while avoiding the use of solvents and making purification steps obsolete.

## 2. Results and Discussion

### 2.1. Assessment of the electrical conductivity

We infiltrated PANI with MoCl<sub>5</sub> and SnCl<sub>4</sub> applying vapor phase infiltration. The process itself is derived from the ALD process, but instead of sequentially exposing the substrate to vapors of two precursors in order to grow a thin film, here we expose the substrate to the vapor of only one precursor and allow sufficient time for the precursor to diffuse into subsurface areas of the substrate. After infiltration, we measured the electrical characteristics of the samples. **Figure 1a,b** shows the room temperature *I-V* characteristics of the fabricated PANI samples. The thicknesses for the samples were comparable and in the range of 7-10 μm. The plots of PANI/1M HCl (black curves) are linear, indicating ohmic behavior over the whole measurement range. Those samples reflect the electrical characteristics of PANI doped

with 1M HCl in a traditional way and serve as reference samples for our new infiltration based doping strategy.

Untreated PANI thin films were measured for reference and showed negligible conductivity ( $\leq 1 \times 10^{-10}$  S/cm). The plots of the infiltrated samples PANI/MoCl<sub>5</sub> (blue curve) and PANI/SnCl<sub>4</sub> (red curve) show linear, **ohmic** behavior in the initial voltage range before changing the slope with the voltage increasing. Two important observations can be made from those two graphs; i) the possibility of using vapor infiltration strategies for doping of PANI is in the first instance an exciting result, which enables many new top-down approaches towards conductive polymers, and ii) thermal treatment of the doped polymers in vacuum has a much lower impact on the conductivity of the metal chloride-doped PANI than on the HCl-doped PANI, indicating a chemical stabilization of the doped polymer. For the forthcoming discussion, we used values for the electrical conductivities of the samples as calculated from the initial slopes of the  $I$ - $V$  plots.

The dramatic enhancement of the conductivity of the PANI films upon infiltrating MoCl<sub>5</sub> or SnCl<sub>4</sub> stands in correlation with the number of infiltration cycles as can be seen in **Figure 1c,d**. Namely, the conductivity of PANI/ MoCl<sub>5</sub> reaches  $8.43 \times 10^{-6}$ ,  $1.75 \times 10^{-4}$ ,  $2.93 \times 10^{-4}$  and  $9.8 \times 10^{-5}$  S/cm after 30, 60, 100, and 200 cycles, respectively, with the highest conductivity being obtained after 100 infiltration cycles. Similarly, the PANI/SnCl<sub>4</sub> films showed conductivities of  $1.17 \times 10^{-6}$ ,  $5.58 \times 10^{-6}$ ,  $1.03 \times 10^{-5}$ , and  $8.26 \times 10^{-6}$  S/cm after 10, 30, 60 and 100 cycles, respectively, and the highest conductivity being observed after 60 cycles. Doping with 1M HCl results in values of  $8.23 \times 10^{-2}$  S/cm, which is clearly better performing. However, this applies to room temperature handling only. **After heating the samples at 150 °C in N<sub>2</sub> at ambient pressure for 100min, we observed that the conductivity of PANI/1M HCl decreased by nearly 3 orders of magnitude from  $8.23 \times 10^{-2}$  S/cm to  $1.06 \times 10^{-4}$  S/cm, while the conductivity of the metal chloride infiltrated samples decreased by a much lower extent, namely from  $1.03 \times 10^{-5}$  S/cm to  $5.05 \times 10^{-6}$  S/cm in the case of PANI/SnCl<sub>4</sub> and from  $2.93 \times$**

$10^{-4}$  S/cm to  $1.45 \times 10^{-4}$  S/cm in the case of PANI/MoCl<sub>5</sub> (**Figure S1**, supporting information).

Furthermore, **Figure 1e** shows that an exposure of the samples to the same elevated temperature, but in vacuum environment for 100 min the conductivities of PANI/MoCl<sub>5</sub> (100 cycles,  $2.07 \times 10^{-5}$  S/cm) and PANI/SnCl<sub>4</sub> (60 cycles,  $3 \times 10^{-6}$  S/cm) clearly outperform the conductivity of PANI/1M HCl ( $8.19 \times 10^{-8}$  S/cm).

## 2.2. FTIR Spectroscopy

The analysis of the various samples by FT-IR (**Figure 2**) shows that the HCl-doped or metal chloride-infiltrated samples drastically differ in their chemistry. Doping with 1M HCl (red spectrum in **Figure 2a**) is severely modifying the signature of PANI (black) before exposure to vacuum and elevated temperatures, but closely resembles the reference spectrum after the thermal and vacuum treatment (**Figure 2b**). This indicates that the thermal and vacuum treatment revert the chemical changes that were induced upon doping. The emeraldine base form of PANI is initially protonated with HCl to form the emeraldine salt, which is stabilized with the Cl<sup>-</sup> ion. Elevated temperatures and vacuum reverse this process and deprotonate the salt to form volatile HCl and the emeraldine base. This results in a loss of conductivity. The spectra of the infiltrated samples on the other hand show a somewhat different behavior. In contrast to the HCl-doped sample, they remain similar to the control sample after doping and only very minor changes are observed upon post-treatment. From the overview in Table 1 one can see that the peak at  $1167 \text{ cm}^{-1}$  in the control sample (in plane C-H bending) has significantly red-shifted to  $1105 \text{ cm}^{-1}$  in PANI/1M HCl, while the red-shift in PANI/SnCl<sub>4</sub> and PANI/MoCl<sub>5</sub> is less significant. This peak is considered as the electronic-like band,<sup>[27]</sup> a measure for the degree of delocalization of electrons in the PANI chains, and thus it is characteristic for its conductivity. The peak at  $1592 \text{ cm}^{-1}$  in PANI is assigned to the quinoid C=C stretching vibration and is a signature of the conversion of quinoid rings to benzenoid rings.<sup>[28]</sup> Similar to above, this peak red-shifted more significantly for the 1M HCl doped

sample than for the metal chloride doped ones. The peak at  $829\text{ cm}^{-1}$ , (out-of-plane C-H deformation of 1,4-disubstituted aromatic rings) red-shifted similarly strong for the 1M HCl and the  $\text{MoCl}_5$  sample and less for the  $\text{SnCl}_4$  sample. The peak at  $1216\text{ cm}^{-1}$ , associated to the C-N stretching vibration, showed a more pronounced shift with both metal chlorides than with HCl. Those observations indicate that HCl is efficiently protonating the polymer chain and converting quinoid rings to benzenoid rings. The chemistry will be different for the metal chloride doped polymer. Given that the process occurs in vacuum and without solvents, no protons are available for protonation, but rather an oxidative doping by a complexation reaction can be assumed. The bulkier molecules will result in a lower doping efficiency due to steric hindrance, which is indicated by the lower shift of the peaks associated to the quinoid stretching modes in comparison to the HCl doped ones. The main difference between the two metal chloride doped polymer samples is seen in the shift of the C-H out plane deformation signals. While HCl and  $\text{MoCl}_5$  doped PANI show similar shifts,  $\text{SnCl}_4$  doped PANI is much closer to the undoped sample, which indicates a less pronounced alteration of the electronic structure of the aromatic sections of the polymer backbone and may be indicative of the measured lower conductivity of the  $\text{SnCl}_4$  doped PANI. However, in spite of the lower conductivity than HCl doped PANI at ambient temperatures, the metal chloride doped PANI outperforms the acid counterpart in terms of stability. As can be seen in **Figure 2b**, after heating at  $150\text{ }^\circ\text{C}$  in vacuum for 100 min, most of the peaks in the PANI/1M HCl spectrum have largely recovered to closely resemble the control sample. On the other hand, the FT-IR spectra of PANI/ $\text{SnCl}_4$  and PANI/ $\text{MoCl}_5$  show only negligible changes.

### 2.3. Raman Spectroscopy

For gaining deeper insight into the material, the prepared samples were further characterized by Raman spectroscopy. **Figure 3** shows the 532 nm laser-excited Raman spectra of PANI,

PANI/1M HCl, PANI/SnCl<sub>4</sub> and PANI/MoCl<sub>5</sub> coated on glass substrates. The laser power was in all cases kept below 0.7 mW at the samples, and the integration times were controlled below 30s for each of the samples, aiming at avoiding structural change which may be caused by extended and strong photo excitation.<sup>[29, 30]</sup>

Table 2 shows that the band at 1592 cm<sup>-1</sup> (C=C stretching of quinoid units) in the PANI reference shifted to higher wavenumbers after doping with either of the three chlorides. The further bands observed at 1336 cm<sup>-1</sup>, 1345 cm<sup>-1</sup> and 1350 cm<sup>-1</sup> are characteristic of all doped samples. Those are assigned to the radical cation (C-N<sup>+</sup> stretching)<sup>[29,30]</sup> and are a result of the protonation of PANI with HCl or the oxidation of PANI after complexation with SnCl<sub>4</sub> or MoCl<sub>5</sub>. Those peaks are not observable in the spectrum of PANI and are only expected when quinoid rings become converted to benzenoid rings. The coordinative interaction of the polymer backbone with the SnCl<sub>4</sub> or MoCl<sub>5</sub> must lower the electron density on the N atoms, and thus a partially positive charge is imposed on the N atoms. A further obvious change relates to the 1491 cm<sup>-1</sup> band in PANI, which is assigned to the C=N stretching of the quinoid units, which is significantly shifting in PANI/SnCl<sub>4</sub> (1496 cm<sup>-1</sup>) and PANI/MoCl<sub>5</sub> (1506 cm<sup>-1</sup>), indicative of a decrease of the amount of quinoid units in the PANI chain. The 1219 cm<sup>-1</sup> band of the benzenoid C-N stretching in PANI also shifted to higher values with all three chlorides. Moreover, the 1418 cm<sup>-1</sup> band of the quinoid C-C stretching in PANI shifted to a higher wavenumber in PANI/1M HCl (1420 cm<sup>-1</sup>), but to a lower wavenumber in PANI/SnCl<sub>4</sub> (1410 cm<sup>-1</sup>) and in PANI/MoCl<sub>5</sub> (1408 cm<sup>-1</sup>). However, the origin of this change is not clear to us at the present. Additionally, a blue shift of the 1167 cm<sup>-1</sup> band in PANI after all three doping approaches should be noted, which is assigned to the in-plane C-H bending of quinoid units.<sup>[31]</sup> After heating the samples at 150 °C for 100 min in vacuum, the most pronounced change in the PANI/1M HCl spectrum is the recovery of the intensity of the peak at 1492 cm<sup>-1</sup>. Generally, the spectrum of the HCl-doped thermally treated PANI resembles closely the

spectrum of the control sample as can be seen in **Figure 4b**. Again, this indicates a recovery of most of the quinoid parts of the molecule, induced by deprotonation of the imine and evaporation of HCl. On the other hand, the Raman spectra of PANI/SnCl<sub>4</sub> and PANI/MoCl<sub>5</sub> show only very minor changes upon thermal treatment in vacuum. The more pronounced shifts of Raman peaks in PANI/MoCl<sub>5</sub> and PANI/SnCl<sub>4</sub> compared to PANI/1M HCl demonstrate that instead of an acid doping possibly complexation reactions between Sn or Mo and N atoms play a more significant role in the evolution of conductive PANI upon vapor phase infiltration.

#### 2.4. SEM and EDX

The morphologies of the samples were examined by SEM and elemental analysis was done by EDX. **Figures 4a-c** shows SEM images of thin films of PANI nanofibers, PANI/MoCl<sub>5</sub> (100 cycles) nanofibers, and PANI/SnCl<sub>4</sub> (60 cycles) nanofibers, which were deposited on the glass wafers. The infiltration did not alter the morphology of the PANI, thus the process can indeed be used for top-down infiltration after a desired morphology of PANI has been obtained. The infiltration process is based on exposure sequences of the PANI substrate to vapors of metal chlorides, which stands in contrast to the traditional coating procedure by ALD, where a counter precursor is used to fabricate a thin layer of a metal oxide. **Figures 4d-f** shows EDX spectra of PANI, PANI/MoCl<sub>5</sub>, and PANI/SnCl<sub>4</sub>, upon thermal treatment at 150 °C in vacuum for 100 min. Peaks stemming from N, Cl, and Mo or Sn can be clearly observed, which confirms that the infiltrated metal chlorides are trapped within the structure and remain there even upon treatment in a harsher environment. Quantitative characterization revealed that after heating in vacuum, the dopant concentration reduced seriously from 13.39 wt% to 1.78 wt% in the case of HCl doped PANI, while the concentration decrease in the metal chloride infiltrated samples was significantly lower, namely from 22.87 wt% to 20.42 wt% in the case of SnCl<sub>4</sub>, and from 26.37 wt% to 24.95 wt% in the case of MoCl<sub>5</sub>. The significantly lower

change in concentration as observed from the metal chlorides doped samples indicates a tight interaction of the precursors with the backbone of the polymer and stabilization of the dopant in a chemical way, presumably through complexation with the nitrogen of the polymer.

## 2.5. Potential Reaction Schemes

Considering the spectroscopic data presented above and publications that reported on various doping strategies of PANI with Lewis acids <sup>[14,15,32]</sup> and transition metal salts, <sup>[16,17]</sup> we propose a reaction scheme as depicted in **Figure 5**. The initial structure of the emeraldine base of PANI contains both amine (-NH) units and imine (=N) units, which act as functional groups for binding MoCl<sub>5</sub> or SnCl<sub>4</sub>. From the Raman spectra we see that the C-N<sup>+</sup> stretching signals are very pronounced, the benzenoid C-N stretching signals shift significantly and the peak intensity of the quinoid C=N stretching signals significantly decrease after the infiltration process. This indicates that the insertion of MoCl<sub>5</sub> and SnCl<sub>4</sub> into the PANI matrix oxidizes the nitrogen partially and binds to the polymer coordinatively. PANI is a hole transporter and upon VPI doping, which will create the positive polarons, the carrier density increase, resulting in increased conductivity. From the UV-Vis spectra of **Figure S2** (supporting information) we observe that on the one hand the band intensity at 336nm decreases, while simultaneously the band intensity at 452nm increases after both doping processes. Those signatures correspond to the  $\pi$ - $\pi^*$  transitions in the benzenoid rings and indicate a stronger presence of benzenoid units. The band at 626nm, which corresponds to the quinoid rings, nearly disappears as a result of the conversion of quinoid rings. The latter can be considered as a signature of polaron. Upon thermal treatment in vacuum, the conductivity decreases, which is a result of the deprotonation of the polymer and evaporation of HCl. The conductivity of PANI/1M HCl is consequently minimized. Only a minor decrease in conductivity is observed after thermal treatment of PANI/MoCl<sub>5</sub> and PANI/SnCl<sub>4</sub> in vacuum. The metal chloride bound to the PANI backbone will resist the thermal treatment, since the

bonding of the metal to the nitrogen will stabilize the metal chloride and prevent its evaporation. The low vapor pressure of the metal chlorides compared to HCl is further supporting the chemical stabilization of the doped polymer.

### 3. Conclusion

In conclusion, we successfully demonstrated a novel way of doping polyaniline by applying an ALD-derived single precursor vapor phase infiltration and doping process. In this way we are able to not only induce conductivity in PANI, but also tune the conductivity through the choice and infiltrated amount of the vaporized precursor. More importantly, the conductivity of the PANI doped in our way was barely affected by a thermal treatment at 150 °C in vacuum, while the conductivity of the acid doped PANI (with 1 M HCl) was almost completely lost. This loss is likely due to a deprotonation of the doped polymer and evaporation of HCl, which results in recovery of the non-conductive emeraldine base of PANI. Doping with MoCl<sub>5</sub> or SnCl<sub>4</sub> on the other hand results in an oxidation of the PANI and presumably in complexation of the metal chlorides with the PANI nitrogen. As a result, the electron mobility along the polymer chains is significantly enhanced and the structure is stabilized even at elevated temperatures. The results are not only significant for the novel process to dope PANI and obtain better thermal stability of the doped polymer, but also for the possibility to perform top-down doping of already manufactured PANI, which allows for better shaping of the material and therefore more efficient device fabrication. The results further encourage future work, particularly the adaptation of similar infiltration processes to more challenging conductive polymers, including polypyrrole or polythiophene.

### 4. Experimental Section

*Synthesis of Polyaniline Nanofibers:* The synthesis of PANI nanofibers was carried out by a rapid mixing polymerization as reported in literature.<sup>[9]</sup> All chemicals were analytical grade

and were used as received. Typically, an aqueous solution of aniline (3.2 mmol) in HCl (1 M, 10 mL) and a solution of ammonium peroxydisulfate (0.8 mmol) in HCl (1 M, 10 mL) were prepared. The two solutions were mixed at room temperature and rapid and immediate shaking ensured efficient mixing. After 12 h polymerization time, the resulting HCl (1 M) doped PANI was collected by filtration and washed several times with HCl (1 M) until the filtrate became colorless. At last, it was dried in vacuum at 50 °C. De-doped PANI was obtained upon treatment of the PANI/1M HCl with aqueous ammonium hydroxide (0.1 M) for 1 h and subsequent washing with deionized water until the filtrate became pH-neutral, and finally dried in vacuum at 60 °C. Glass substrates (1.3×1.3 cm<sup>2</sup>) were cleaned in sequence with acetone, deionized water (DI), and isopropanol, and subsequently dried in an oven overnight. PANI and PANI/1M HCl films were coated (200 μL) on the glass substrates and the samples were dried in an oven at 60 °C for 12 h. In advance of the infiltration experiments, the de-doped PANI films were stored overnight at 120 °C.

*Vapor-phase Infiltration Process:* Vapor-phase infiltration was performed using a homemade atomic layer deposition tool. De-doped PANI films on glass substrates were exposed to vapors of SnCl<sub>4</sub> (Sigma, 98%) or MoCl<sub>5</sub> (Sigma, 95%) in a pulse-exposure-purge sequence with varied numbers of repetition cycles. One cycle of the process consisted of following settings: the precursors were pulsed into the reaction chamber for 0.1 s (SnCl<sub>4</sub>) or 5 s (MoCl<sub>5</sub>) and exposure of the substrates to the vapors in the reaction chamber was allowed for 120 s. The exposure was followed by a 60 s purge step. The cycle was repeated with the number of cycles varying between 10 and 200. As carrier and purging gas N<sub>2</sub> (99.99%) was used. The reaction temperature was 150 °C, and the base pressure of the reactor was ~50 mTorr. Since at room temperature MoCl<sub>5</sub> is solid, heating of that precursor to 85 °C was required to obtain reasonable vapor pressure.

*Characterization:* Infrared spectra of the samples were recorded between 700 and 1800 cm<sup>-1</sup> with a FTIR Spectrometer (PerkinElmer, Frontier). The morphology of the samples was characterized by scanning electron microscopy (FEI, Quanta 250 FEG) and the composition with energy-dispersive X-ray spectroscopy (EDX). Thickness measurements were done with cross-sectional FEG-SEM. Raman spectra at 532 nm exciting wavelength were collected with a Raman microscope (Alpha 300S, WITec). The laser power was kept below 0.7 mW in order to avoid sample degradation. Absorption spectra of the samples were recorded between 250-880 nm using a UV-vis spectrophotometer (V-630 BIO, JASCO). The conductivities of the films were measured applying a four-point probe technique with a source measurement unit (Keithley 2611). The resulting conductivity,  $\sigma$ , was calculated according to the formula,

$$\sigma = \ln 2(I/\pi dV) \quad (1)$$

where  $I$  is the current,  $V$  is the voltage and the  $d$  is the film thickness.

## Acknowledgements

The authors acknowledge the funding from European Union FP7 Programme under grant agreement n°607232 [MARIE-CURIE-ITN THINFACE], and the work is performed with the PCAM European doctorate. M.K. acknowledges financial support by the Basque government through the project number PI2013-56 and the EU-FP7 program through Marie Curie Actions (CIG) within grant agreement n°322158 (ARTEN).

Received: ((will be filled in by the editorial staff))

Revised: ((will be filled in by the editorial staff))

Published online: ((will be filled in by the editorial staff))

- [1] H. Klauk, *Chem. Soc. Rev.* **2010**, *39*, 2643.
- [2] Y. Yang, E. Westerweele, C. Zhang, P. Smith, A. J. Heeger, *J. Appl. Phys.* **1995**, *77*, 694.
- [3] J. Y. Kim, K. Lee, N. E. Coates, D. Moses, T. Nguyen, M. Dante, A. J. Heeger, *Science* **2007**, *317*, 222.
- [4] H. K. Song, G. T. R. Palmore, *Adv. Mater.* **2006**, *18*, 1764.
- [5] Q. Wu, Y. Xu, Z. Yao, A. Liu, G. Shi, *ACS Nano* **2010**, *4*, 1963.
- [6] D. Li, J. X. Huang, R. B. Kaner, *Acc. Chem. Res.* **2009**, *42*, 135.
- [7] L. J. Pan, G. H. Yu, D. Y. Zhai, H. R. Lee, W. T. Zhao, N. Liu, H. L. Wang, B. C. K. Tee, Y. Shi, Y. Cui, Z. N. Bao, *Proc. Natl. Acad. Sci. USA.* **2012**, *109*, 9287.
- [8] S. H. Lee, D. H. Lee, K. Lee, C. W. Lee, *Adv. Funct. Mater.* **2005**, *15*, 1495.
- [9] J. X. Huang, R. B. Kaner, *Angew. Chem. Int. Ed.* **2004**, *43*, 5817.
- [10] D. Das, A. Datta, A. Q. Contractor, *J. Phys. Chem. B* **2014**, *118*, 12993.
- [11] J. Stejskal, I. Sapurina, M. Trchova, J. Prokes, *Chem. Mater.* **2002**, *14*, 3602.
- [12] K. S. Ryu, B. W. Moon, J. Joo, S. H. Chang, *Polymer.* **2001**, *42*, 9355.
- [13] S. A. Chen, L. C. Lin, *Macromolecules* **1995**, *28*, 1239.
- [14] I. K. Bajer, A. Pron, J. Abramowicz, C. Jeandey, J. L. Oddou, J. W. Sobczak, *Chem. Mater.* **1999**, *11*, 552.
- [15] D. Chaudhuri, A. Kumar, I. Rudra, D. D. Sarma, *Adv. Mater.* **2001**, *13*, 1548.
- [16] O. P. Dimitriev, *Macromolecules* **2004**, *37*, 3388.
- [17] C. M. S. Izumi, A. M. D. C. Ferreira, V. R. L. Constantino, M. L. A. Temperini, *Macromolecules* **2007**, *40*, 3204.
- [18] K. E. Gregorczyk, M. Knez, *Progress in Materials Science* **2016**, *75*, 1.
- [19] I. Manners, *Science* **2001**, *294*, 1664.
- [20] C. Sanchez, B. Julián, P. Belleville, M. Popall, *J. Mater. Chem.* **2005**, *5*, 3559.
- [21] R. Houbertz, G. Domann, J. Schulz, B. Olsowski, L. Fröhlich, W. S. Kim, *Appl. Phys. Lett.* **2004**, *84*, 1105.

- [22] M. J. MacLachlan, M. Ginzburg, N. Coombs, T. W. Coyle, N. P. Raju, J. E. Greendan, G. A. Ozin, I. Manners, *Science* **2000**, *287*, 1460.
- [23] S. M. Lee, V. Ischenko, E. Pippel, A. Masic, O. Moutanabbir, P. Fratzl, M. Knez. *Adv. Funct. Mater.* **2011**, *21*, 3047.
- [24] S. M. Lee, E. Pippel, U. Gösele, C. Dresbach, Y. Qin, C. V. Chandran, T. Bräuniger, G. Hause, M. Knez, *Science*, **2009**, *324*, 488.
- [25] S. M. Lee, E. Pippel, O. Moutanabbir, I. Gunkel, T. Thurn-Albrecht, M. Knez, *ACS Appl. Mater. Interfaces* **2010**, *2*, 2436.
- [26] K. E. Gregorczyk, D. F. Pickup, M. G. Sanz, I. A. Irakulis, C. Rogero, M. Knez. *Chem. Mater.* **2015**, *27*, 181.
- [27] W.R. Salaneck, B. Liedberg, O. Inganäs, R. Erlandsson, I. Lundström, A.G. MacDiarmid, M. Halpern, N.L.D. Somasiri, *Mol. Cryst. Liq. Cryst.* **1985**, *121*, 191.
- [28] Y. H. Kim, C. Foster, J. Chiang, A. J. Heeger, *Synth. Met.* **1988**, *26*, 49.
- [29] T. Fukuda, H. Takezoe, K. Ishikawa, A. Fukuda, H. S. Woo, S. K. Jeong, E. J. Oh, J. S. Suh, *Synth. Met.* **1995**, *69*, 175.
- [30] J. E. Pereira da Silva, S. I. Cordoba de Torresi, D. L. A. De Faria, M. L. A. Temperini, *Synth. Met.* **1999**, *101*, 834.
- [31] G. Louarn, M. Lapskowski, S. Quillard, A. Pron, J. P. Buisson, S. Lefrant, *J. Phys. Chem.* **1996**, *100*, 6998.
- [32] F. Genoud, I. K. Bajer, A. Bedel, J. L. Oddou, C. Jeandey, A. Pron, *Chem. Mater.* **2000**, *12*, 744.

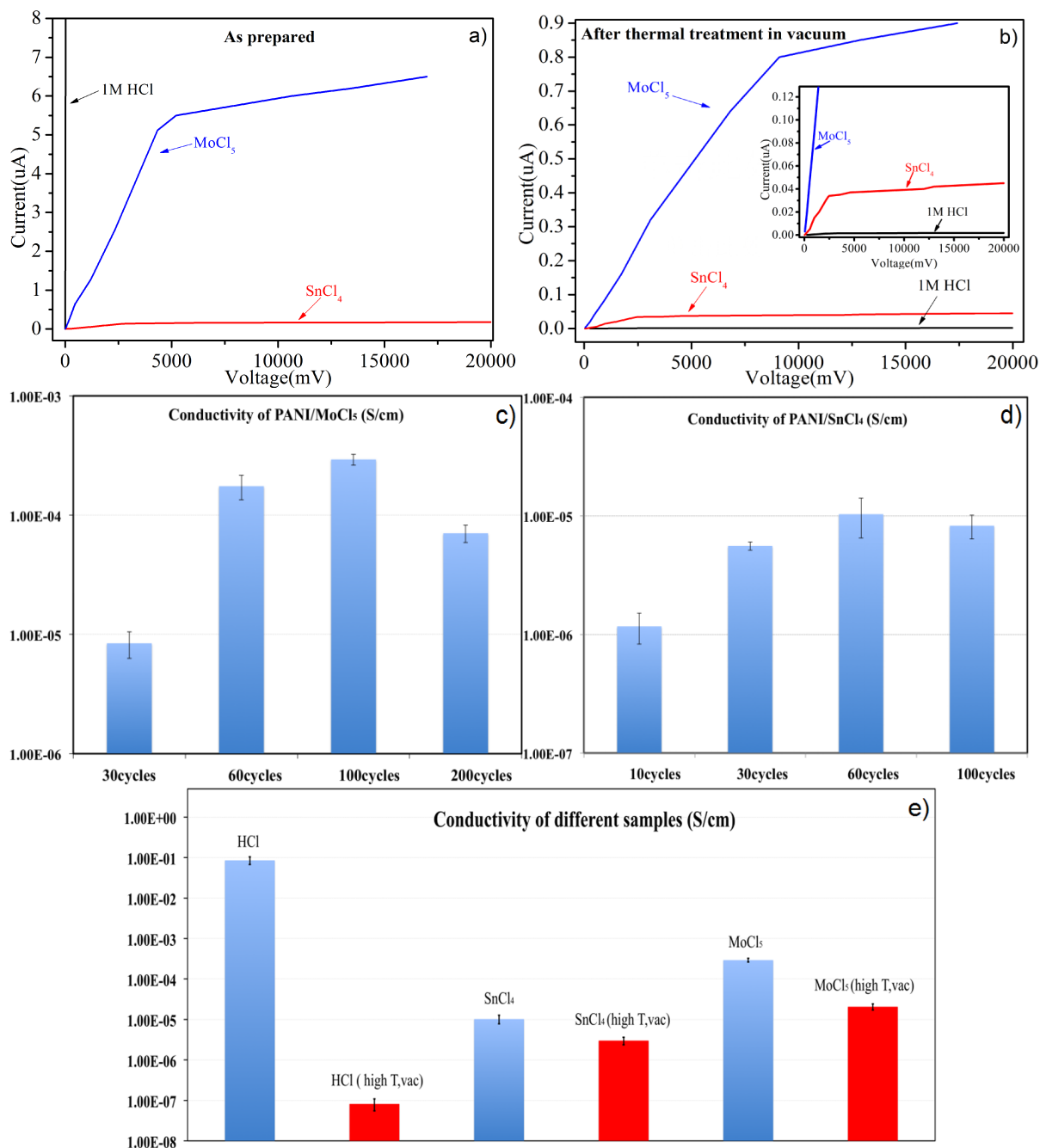


**Figure 1.** *I-V* plots of (a) PANI/1M HCl, PANI/MoCl<sub>5</sub> (100 cycles) and PANI/SnCl<sub>4</sub> (60 cycles) as prepared and (b) PANI/1M HCl, PANI/MoCl<sub>5</sub> (100 cycles) and PANI/SnCl<sub>4</sub> (60 cycles) after storage at 150 °C in vacuum for 100 min. The inset shows the low current range area of Figure 1b. Conductivities of (c) MoCl<sub>5</sub> and (d) SnCl<sub>4</sub> as a function of the number of infiltration cycles (measured at room temperature). (e) Conductivity comparison of PANI/1M HCl, PANI/SnCl<sub>4</sub> (60 cycles) and PANI/MoCl<sub>5</sub> (100 cycles) as prepared, and after storage at 150 °C in vacuum for 100 min.

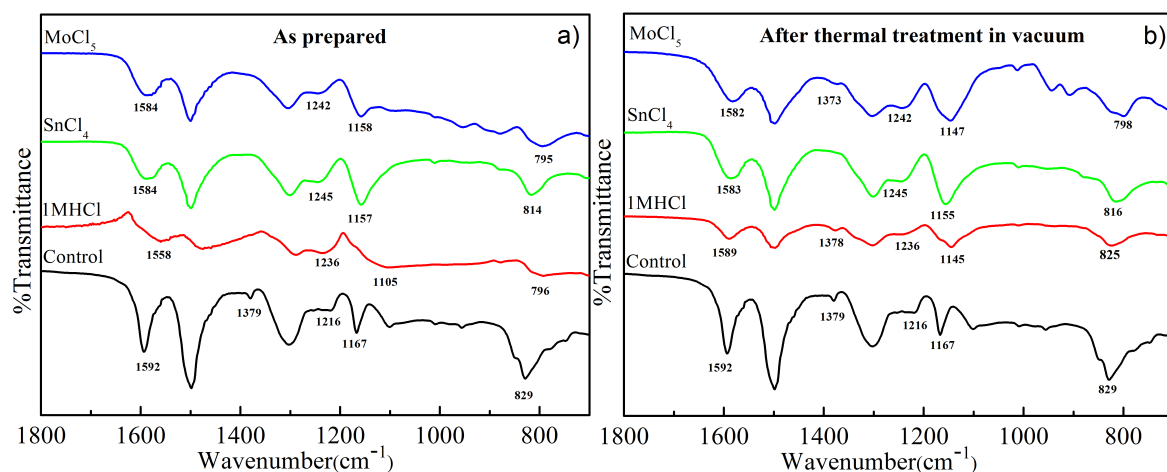


**Figure 2.** FT-IR spectra of undoped PANI (Control), PANI/1M HCl, PANI/SnCl<sub>4</sub> (60 cycles) and PANI/MoCl<sub>5</sub> (100 cycles), before (a) and after (b) treatment at 150 °C in vacuum environment for 100 min.

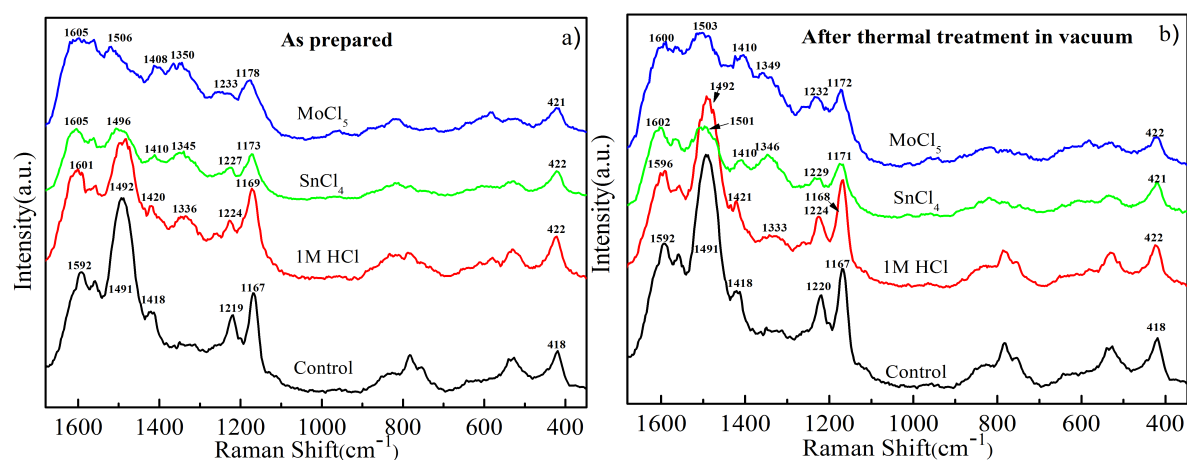


**Figure 3.** Raman spectra of PANI showing the 1680-350 cm<sup>-1</sup> region (a) Control, PANI/1M HCl, PANI/SnCl<sub>4</sub> (60 cycles) and PANI/MoCl<sub>5</sub> (100 cycles), (b) Control, PANI/1M HCl, PANI/SnCl<sub>4</sub> (60 cycles) and PANI/MoCl<sub>5</sub> (100 cycles) under high temperature (150 °C), vacuum environment for 100 min.

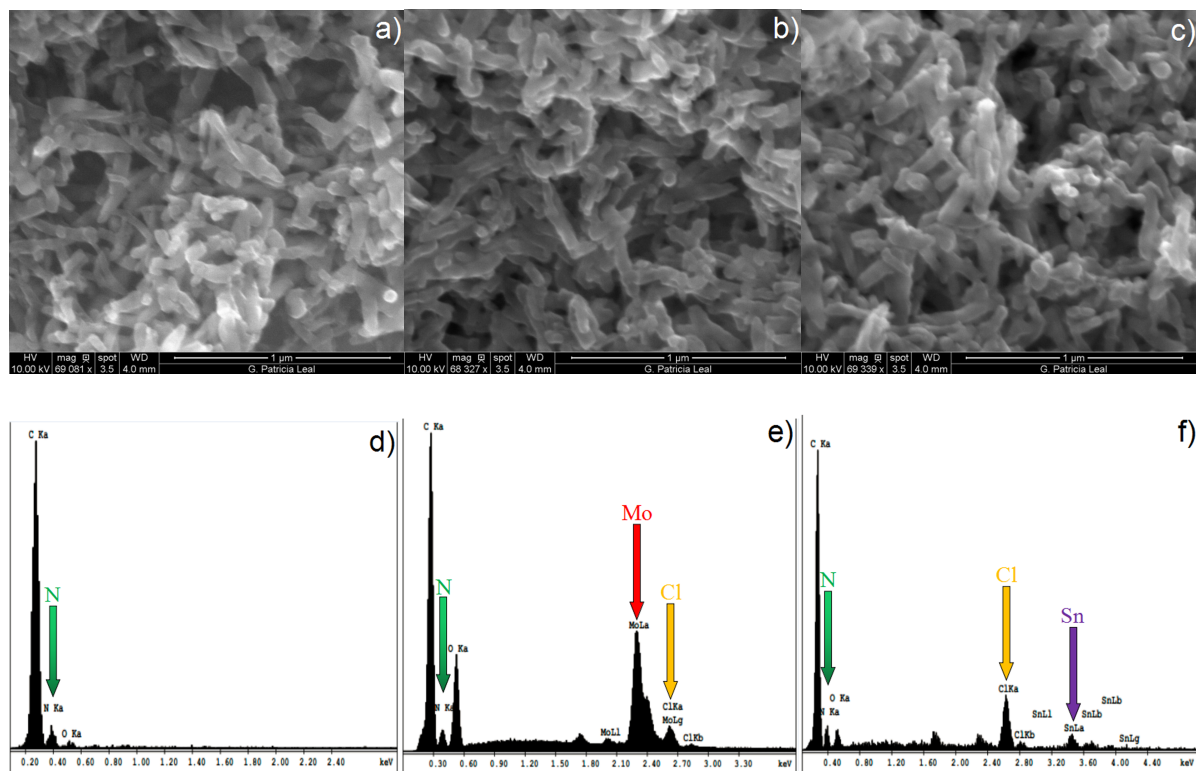


**Figure 4.** SEM images of (a) PANI nanofiber, (b) PANI/MoCl<sub>5</sub> (100 cycles) nanofiber thin film, and (c) PANI/SnCl<sub>4</sub> (60 cycles) nanofiber thin film; EDX spectra of (d) PANI, (e) PANI/MoCl<sub>5</sub>, (f) PANI/SnCl<sub>4</sub>, after thermal treatment at 150 °C in vacuum for 100 min.

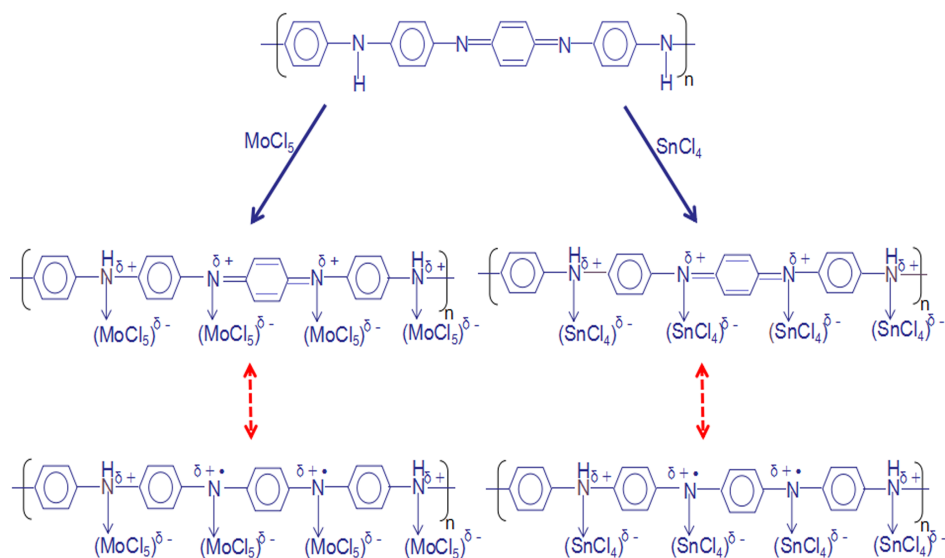


**Figure 5.** Proposed structures of PANI/MoCl<sub>5</sub> and PANI/SnCl<sub>4</sub> after infiltration of PANI with MoCl<sub>5</sub> or SnCl<sub>4</sub>.

**Table 1.** Overview of the most characteristic peaks in the FT-IR spectra in the 1800-700 $\text{cm}^{-1}$  region of PANI and PANI doped with 1M HCl,  $\text{SnCl}_4$  and  $\text{MoCl}_5$  measured before and after thermal treatment (150 °C) in vacuum for 100 min.

	PANI	PANI/1M HCl	PANI/ $\text{SnCl}_4$	PANI/ $\text{MoCl}_5$
In plane C-H bending	1167 $\text{cm}^{-1}$	As prepared 1105 $\text{cm}^{-1}$	1157 $\text{cm}^{-1}$	1158 $\text{cm}^{-1}$
C=C stretching (quinoid)	1592 $\text{cm}^{-1}$	1558 $\text{cm}^{-1}$	1584 $\text{cm}^{-1}$	1584 $\text{cm}^{-1}$
Out plane C-H bending	829 $\text{cm}^{-1}$	796 $\text{cm}^{-1}$	814 $\text{cm}^{-1}$	795 $\text{cm}^{-1}$
C-N stretching	1216 $\text{cm}^{-1}$	1236 $\text{cm}^{-1}$	1245 $\text{cm}^{-1}$	1242 $\text{cm}^{-1}$
After thermal treatment in vacuum				
In plane C-H bending	1167 $\text{cm}^{-1}$	1145 $\text{cm}^{-1}$	1155 $\text{cm}^{-1}$	1147 $\text{cm}^{-1}$
C=C stretching (quinoid)	1592 $\text{cm}^{-1}$	1589 $\text{cm}^{-1}$	1583 $\text{cm}^{-1}$	1582 $\text{cm}^{-1}$
Out plane C-H bending	829 $\text{cm}^{-1}$	825 $\text{cm}^{-1}$	816 $\text{cm}^{-1}$	798 $\text{cm}^{-1}$
C-N stretching	1216 $\text{cm}^{-1}$	1236 $\text{cm}^{-1}$	1245 $\text{cm}^{-1}$	1242 $\text{cm}^{-1}$

**Table 2.** Overview of the most characteristic peaks in the Raman spectra in the 1680-350 $\text{cm}^{-1}$  region of PANI and PANI doped with 1M HCl,  $\text{SnCl}_4$  and  $\text{MoCl}_5$  measured before and after thermal treatment (150 °C) in vacuum for 100 min.

	PANI	PANI/1M HCl	PANI/ $\text{SnCl}_4$	PANI/ $\text{MoCl}_5$
C=C stretching (quinoid)	1592 $\text{cm}^{-1}$	As prepared 1601 $\text{cm}^{-1}$	1605 $\text{cm}^{-1}$	1605 $\text{cm}^{-1}$
C-N <sup>+</sup> stretching	--	1336 $\text{cm}^{-1}$	1345 $\text{cm}^{-1}$	1350 $\text{cm}^{-1}$
C=N stretching (quinoid)	1491 $\text{cm}^{-1}$	1492 $\text{cm}^{-1}$	1496 $\text{cm}^{-1}$	1506 $\text{cm}^{-1}$
C-C stretching (quinoid)	1418 $\text{cm}^{-1}$	1420 $\text{cm}^{-1}$	1410 $\text{cm}^{-1}$	1408 $\text{cm}^{-1}$
C-N stretching (benzenoid)	1219 $\text{cm}^{-1}$	1224 $\text{cm}^{-1}$	1227 $\text{cm}^{-1}$	1233 $\text{cm}^{-1}$
In plane C-H bending (quinoid)	1167 $\text{cm}^{-1}$	1169 $\text{cm}^{-1}$	1173 $\text{cm}^{-1}$	1178 $\text{cm}^{-1}$
After thermal treatment in vacuum				
C=C stretching (quinoid)	1592 $\text{cm}^{-1}$	1596 $\text{cm}^{-1}$	1602 $\text{cm}^{-1}$	1600 $\text{cm}^{-1}$
C-N <sup>+</sup> stretching	--	1333 $\text{cm}^{-1}$	1346 $\text{cm}^{-1}$	1349 $\text{cm}^{-1}$
C=N stretching (quinoid)	1491 $\text{cm}^{-1}$	1492 $\text{cm}^{-1}$	1501 $\text{cm}^{-1}$	1503 $\text{cm}^{-1}$
C-C stretching (quinoid)	1418 $\text{cm}^{-1}$	1421 $\text{cm}^{-1}$	1410 $\text{cm}^{-1}$	1410 $\text{cm}^{-1}$
C-N stretching (benzenoid)	1220 $\text{cm}^{-1}$	1224 $\text{cm}^{-1}$	1229 $\text{cm}^{-1}$	1232 $\text{cm}^{-1}$
In plane C-H bending (quinoid)	1167 $\text{cm}^{-1}$	1168 $\text{cm}^{-1}$	1171 $\text{cm}^{-1}$	1172 $\text{cm}^{-1}$